Glutathione reductase deficiency alters lung development and hyperoxic responses in neonatal mice

Mary E. Robbins [a],[*],[1],[2], Hye-Youn Cho [b],[1], Jason M. Hansen [c], Joseph R. Luchsinger [d], Morgan L. Locy [e], Markus Velten [f], Steven R. Kleeberger [b], Lynette K. Rogers [g], Trent E. Tipple [h]

[a] *Division of Neonatology, Department of Pediatrics, Northwestern University, Chicago, IL, USA*
[b] *Immunity, Inflammation, and Disease Laboratory, National Institute of Environmental Health Sciences, Research Triangle Park, NC, USA*
[c] *Physiology & Developmental Biology, Brigham Young University, Provo, UT, USA*
[d] *Medical Scientist Training Program, Vanderbilt University, Nashville, TN, USA*
[e] *Medical Scientist Training Program, University of Alabama at Birmingham, Birmingham, AL, USA*
[f] *Department of Anesthesiology and Intensive Care Medicine, Rheinische Friedrich- Wilhelms University, University Medical Center, Bonn, Germany*
[g] *Center for Perinatal Research, The Research Institute at Nationwide Children's Hospital, Columbus, OH, USA*
[h] *Center for Pregnancy and Newborn Research, Section of Neonatal-Perinatal Medicine, University of Oklahoma Health Sciences Center, Oklahoma City, OK, USA*

ARTICLE INFO

ABSTRACT

Cellular antioxidants protect against hyperoxic lung injury. The role of the glutathione (GSH) system in lung development and bronchopulmonary dysplasia (BPD) pathogenesis has not been systematically investigated. The current study utilized GSH reductase-deficient (*Gsr*-KO) neonatal mice to test the hypothesis that early disruption of the GSH system negatively impacts lung development and hyperoxic responses. Lungs from wild-type (*Gsr*-WT) and *Gsr*-KO mice were analyzed for histopathology, developmental markers, redox indices, and transcriptome profiling at different developmental stages following exposure to room air or hyperoxia (85% O_2) for up to 14 d. Lungs from *Gsr*-KO mice exhibited alveolar epithelial dysplasia in the embryonic and neonatal periods with relatively normal lung architecture in adulthood. GSH and its oxidized form (GSSG) were 50–70% lower at E19-PND14 in *Gsr*-KO lungs than in age-matched *Gsr*-WT. Differential gene expression between *Gsr*-WT and *Gsr*-KO lungs was analyzed at discrete developmental stages. *Gsr*-KO lungs exhibited downregulated cell cycle and DNA damage checkpoint genes at E19, as well as lung lipid metabolism and surfactant genes at PND5. In addition to abnormal baseline lung morphometry, *Gsr*-KO mice displayed a blunted response to hyperoxia. Hyperoxia caused a more robust upregulation of the lung thioredoxin system in *Gsr*-KO compared to *Gsr*-WT. *Gsr*-dependent, hyperoxia-responsive genes were highly associated with abnormal cytoskeleton, skeletal-muscular function, and tissue morphology at PND5. Overall, our data in *Gsr*-KO mice implicate the GSH system as a key regulator of lung development, cellular differentiation, and hyperoxic responses in neonatal mice.

1. Introduction

In preterm infants, oxygen toxicity is a frequent consequence of prolonged supplemental oxygen exposure that contributes to the development of bronchopulmonary dysplasia (BPD) [1,2]. The mechanisms that mediate oxygen-induced lung injury are primarily mediated through the actions of reactive oxygen intermediates including superoxide ($O_2^{\bullet-}$), hydrogen peroxide (H_2O_2), peroxynitrite ($ONOO^-$), and

hydroxyl radical (HO•) [3]. Glutathione (GSH) peroxidases (GPx) catalyze the GSH-dependent reduction of H_2O^2 and other oxidants resulting in the oxidation of GSH to glutathione disulfide (GSSG). Glutathione reductase (GSR) catalyzes the reduction of GSSG to GSH using NADPH as an electron donor ($NADPH + H^+ + GSSG \rightarrow NADP^+ + 2\ GSH$). We and others have shown that *Gsr* deficiency appears to be well tolerated in adult mice [4–9].

Thioredoxin (TXN) is a dithiol/disulfide oxidoreductase that is catalytically maintained in a reduced state by the enzyme thioredoxin reductase (TXNRD). A series of preclinical studies by our group has established pharmacologic TXNRD inhibition as a promising therapeutic strategy to prevent neonatal and adult lung injury [10–15]. Nuclear factor (erythroid-derived 2)-like 2 (NRF2)-mediated upregulation of GSH-dependent antioxidant defenses are necessary for the efficacy of TXNRD inhibitors to prevent lung injury [8,10]. Compensatory upregulation of the TXN system contributes to the resistance of adult *Gsr*-deficient (*Gsr*-KO) mice to hyperoxic lung injury [8].

The role of GSR on lung development and hyperoxic responses in neonatal mice has not been formally investigated. The current study utilized neonatal *Gsr*-KO mice to test the hypothesis that disruption of the GSH system negatively impacts lung development and alters hyperoxia-induced lung injury in neonates.

2. Methods

2.1. Animals, timed mating, and exposure

Animal studies were performed at The Abigail Wexner Research Institute at Nationwide Children's Hospital using protocols approved by the Institutional Animal Care and Use Committee. Wild-type (*Gsr*-WT, C3H/HeN) mice were purchased from Harlan (Indianapolis, IN). *Gsr*-KO mice were generated as described previously [16,17]. Mice were bred and dated as to time of pregnancy. Time-pregnant dams were euthanized at E19 by cervical dislocation and the embryos were removed. For exposure studies, newborn mice were exposed to room air (FiO^2 0.21) or hyperoxia (FiO^2 0.85) beginning within 12 h of life on postnatal day 0.5 (PND 0.5) for up to 14 d. Dams were rotated every 24 h to prevent oxygen toxicity. Pups were weighed daily. Subsets of hyperoxia-exposed mice were returned to room air for up to PND56. In both prenatal and perinatal studies, lungs were harvested at designated times and either inflation fixed with 10% formalin or were snap frozen in liquid nitrogen and stored at −80 °C for molecular analyses.

2.2. Lung glutathione measurements

The concentrations of reduced (GSH) and disulfide (GSSG) forms of glutathione were measured by HPLC and were determined using simultaneously run standard curves [18,19]. Redox potentials of GSSG/GSH [Eh(GSSG/GSH)] were calculated according to the Nernst equation [18].

2.3. Pulmonary function testing

Pulmonary function analyses were performed in adult mice using Flexivent system (Scireq, Montreal, QC, Canada) [20].

2.4. Western blotting

Lungs were homogenized in radioimmunoprecipitation assay (RIPA) buffer. The following antibodies were used: mouse canonical alveolar type 1 cell (AT1) marker T1-alpha (T1α, hamster monoclonal, clone 8.1.1, University of Iowa Hybridoma Bank), alveolar type 2 cell (AT2) cell marker surfactant protein C (SP–C, goat polyclonal, Santa Cruz Biotechnologies, Dallas, TX), and β-actin (goat polyclonal, Santa Cruz Biotechnologies). The membranes were developed with ECL + reagent (GE Healthcare, Buckinghamshire, UK) and read with a phosphoimager

(GE Healthcare, Buckinghamshire, UK) and band images (n=3/group) were quantitated using ImageQuant software (Molecular Dynamics, Sunnyvale, CA).

2.5. Genome-wide transcriptomic analyses

Lungs were collected from *Gsr*-WT and *Gsr*-KO embryos at E19, or from animals exposed to room air (FiO$_2$=0.21) or hyperoxia (FiO$_2$=0.85) from birth to PND5. Lungs were collected from a separate set of animals exposed to room air or hyperoxia from PND0-14 then raised in room air through PND56. RNA was isolated from lung homogenates of each mouse (n = 4/group for embryos, n = 3/group for others) using the RNeasy Mini-Plus kit (Qiagen, Valencia, CA). Aliquots of total lung RNA (200 ng) were applied to mouse 430 2.0 array (Affymetrix, Inc., Santa Clara, CA) in the NIEHS Microarray Core Facility as described previously [21]. Using GeneSpring GX software (Agilent Technologies, Inc., Santa Clara, CA), independent experiments were created using raw data of E19 (*Gsr-WT*, *Gsr-KO*), PND5 (*Gsr-WT/0.21*, *Gsr-WT/0.85*, *Gsr-KO/0.21*, *Gsr-KO/0.85*), and PND56 (*Gsr-WT/0.21*, *Gsr-WT/0.85*, *Gsr-KO/0.21*, *Gsr-KO/0.85*). Array raw data were filtered by lower expression percentile (at least 1 sample had values within 20% cut-off rage) and the expression levels were normalized to mean value of experimental control (i.e., *Gsr-WT* in E19, *Gsr-WT/0.21* in PND5, *Gsr-WT/0.21* in PND56) for each gene by quantile algorithm. Moderated *t*-test (E19/*Gsr-WT* vs E19/*Gsr-WT*, PND5- *Gsr-WT/0.21* vs PND5-*Gsr-WT/0.21*, PND56-*Gsr-WT/0.21* vs PND56- *Gsr-WT/0.21*, PND5-*Gsr-KO/0.21* vs PND5- *Gsr-KO/0.85*) or 2-way ANOVA followed by Student-Newman-Keuls comparison (interaction between genotype and exposure in *Gsr-WT* or in *Gsr-KO* at PND5 and PND56) identified statistically significant genes (*p* value cut-off at < 0.01). Ingenuity Pathway Analysis (IPA, Qiagen Inc., Valencia, CA) predicted underlying molecular mechanisms including upstream modulators and downstream effectors as well as molecular interactions. Microarray data are deposited in Gene Expression Omnibus (GEO, accession number GSE116485).

2.6. Statistical analysis

Non-microarray data were analyzed by unpaired *t*-test or by ANOVA followed by post hoc testing using GraphPad Prism Version 8 (San Diego, CA). Significance was accepted at p < 0.05. Microarray data analysis is described above.

3. Results

3.1. Lung glutathione contents in Gsr-KO mice

Lung GSH and GSSG contents were significantly lower in *Gsr*-KO lungs when compared to age-matched *Gsr*-WT controls at PND0, PND1, PND3, PND7 and PND14 (Fig. 1A and B). In embryonic lungs, GSSG but not GSH contents were lower in *Gsr*-KO vs *Gsr*-WT controls (Fig. 1B). Effects of *Gsr* deletion on lung GSH:GSSG ratios were inconsistent (Fig. 1C). Redox potentials (*Eh*) were calculated using the Nernst equation in order to express the redox potential of the GSH/GSSG thiol/disulfide couple [22]. GSSG/GSH potential was significantly lower (4–13%) in *Gsr*-KO compared to age matched *Gsr*-WT at all embryonic and neonatal timepoints (Fig. 1D).

3.2. Role of GSR in developmental mouse lung

Body weights were not significantly different between *Gsr*-WT and *Gsr*-KO mice between PND0-PND70 (Supplemental Fig. 1). Canalicular stage lungs from *Gsr*-KO mice at E19 display septal thickening and epithelial dysplasia when compared to *Gsr*-WT mice (Fig. 2A). Persistent septal thickening and epithelial cell dysplasia were also evident at PND3 in *Gsr*-KO mice (Fig. 2B). There was little histologic difference between mature *Gsr*-KO and *Gsr*-WT lungs at PND56 (Fig. 2C). Pulmonary
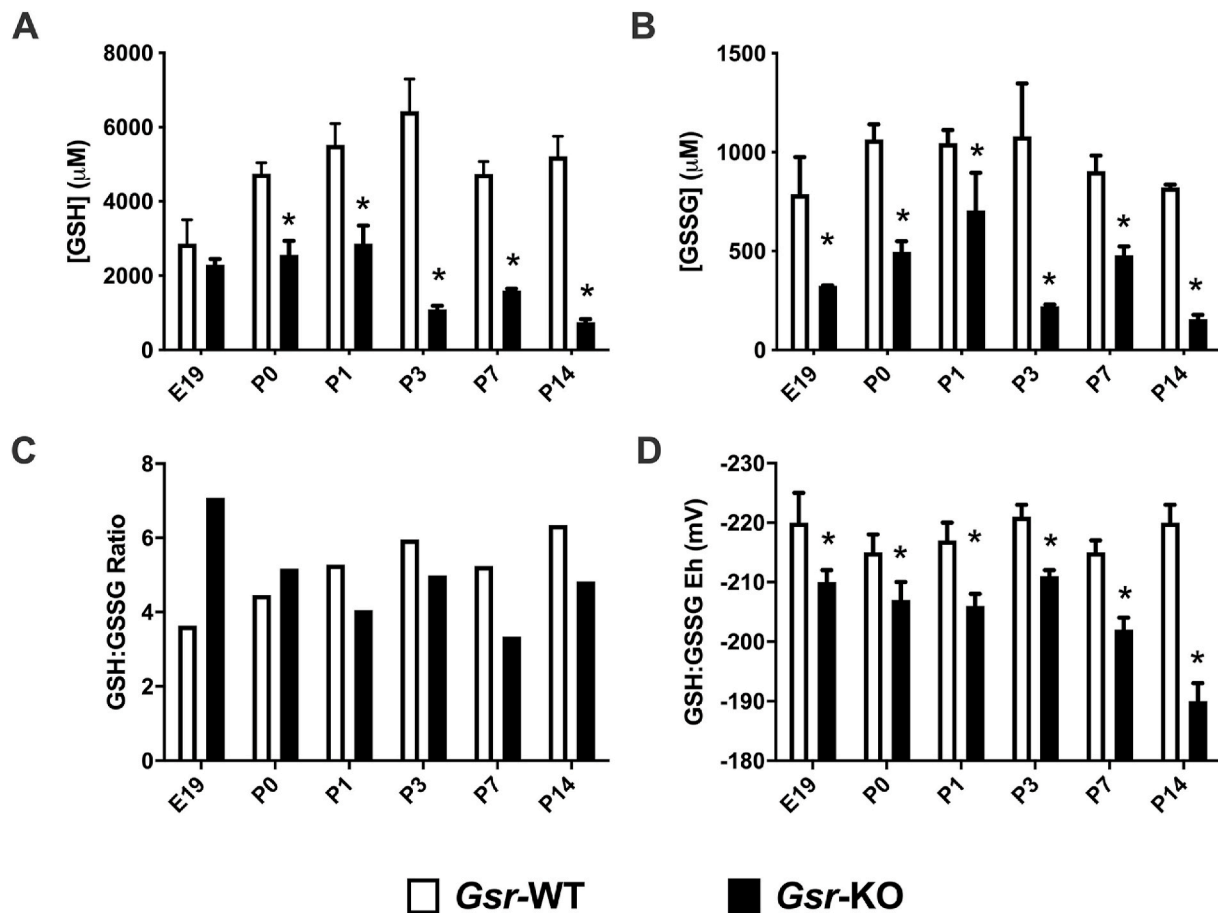
Fig. 1. Lung glutathione contents in embryo and newborn wild-type (*Gsr*-WT) and *Gsr*-deficient (*Gsr*-KO) mice. (A) Independent effects of genotype and day of life as well as interaction on oxidized (GSH) and (B) reduced disulfide (GSSG) glutathione contents were detected in lung homogenates from newborn *Gsr*-WT and *Gsr*-KO mice. (C) GSH/GSSG ratios were subsequently calculated. (D) Calculated GSH redox potential demonstrated independent effects of genotype and day of life as well as interaction between the two. Data are expressed as mean +SEM (*$p < 0.05$ vs *Gsr*-WT, n=3–6) and were analyzed by 2-way ANOVA with Tukey's multiple comparison test.

function analyses revealed baseline differences in adult function between genotypes. *Gsr*-KO mice had decreased pulmonary resistance and total lung capacity compared to *Gsr*-WT mice (Fig. 2D, G), but no difference in airway resistance or compliance (Fig. 2E and F). In addition, *Gsr*-KO exhibited significantly enhanced airway responsiveness to methacholine starting at the 5 mg/ml dosage when compared to *Gsr*-WT (Fig. 2H).

3.3. Lung T1 alpha (T1α) and surfactant protein C (SP–C) expression

To further explore the alveolar cell dysplasia found in *Gsr*-KO mice, western blotting was performed on whole lung homogenates using antibodies for canonical alveolar type 1 cells (AT1; T1α) and alveolar type 2 cells (AT2; SP-C). Lung T1α protein levels increased as a function of age between E19 and PND70 in *Gsr*-WT mice (Fig. 3A). In contrast to findings of increased T1α expression at PND70 in *Gsr*-WT mice, T1α expression in *Gsr*-KO mice did not increase above the levels observed at PND28. There were no consistent differences in SP-C expression in either *Gsr*-WT or *Gsr*-KO mice (Fig. 3B).

3.4. Role of Gsr in developmental lung transcriptomics

Overall, pulmonary transcriptome variation between *Gsr*-WT and *Gsr*-KO mice was more predominant in developing lungs (E19 and PND5) than in mature lungs at PND56 (Fig. 4A). Many of the genes known to have *Gsr*-dependent regulation were highly suppressed (up to

40 fold) in *Gsr*-KO lungs versus *Gsr*-WT lungs at E19 and PND5 [e.g., cytochrome P450, family 2 (e.g., *Cyp2d26*), alpha-2-macroglobulin (*A2m*), apolipoprotein family (e.g., *Apoc2*), serine (or cysteine) peptidase inhibitor, clade A family (e.g., *Serpina1a*), fibrinogen alpha chain (*Fga*), albumin (*Alb*), alpha fetoprotein (*Afp*)] (Tables 1, S1, S2). GSR may play roles in unique pathways at different lung developmental stages, as only a small number of genes were commonly modulated by *Gsr* (black block in Fig. 4A) between canalicular (E19), saccular-alveolar (PND5), and mature lungs (PND56).

In the canalicular lung (E19), *Gsr*-dependent lung transcriptome variation was greatest (Fig. 4A). Among the significantly varied genes (n=908, $p < 0.01$; Tables 1 and S1), a cluster of genes involved in cell cycle control of chromosomal replication and DNA damage checkpoint regulation were suppressed in *Gsr*-KO lungs compared to *Gsr*-WT lungs (Fig. 4B, Table 1). Cell division cycle (e.g., *Cdc6*) and cyclin and related (e.g., *Ccnb1*, *Cdk1*) genes were highly represented (Tables 1 and S1). These data suggest that embryonic *Gsr* deficiency may interrupt cell cycle in the developing lung and may contribute to the histopathologic septal thickening and alveolar epithelial dysplasia observed in *Gsr*-KO lungs at E19 (Fig. 2A). In contrast, *Gsr*-KO embryonic lung had markedly heightened expression of inflammatory and cell death response genes versus *Gsr*-WT (Fig. 4B, Tables 1 and S1). These genes include interferon-induced protein family (*Ifit1*), toll like receptor signal transducers (*Tlr4*, *Cd14*), and complement (*C6*). Several cytochrome P450 (*Cyp2d26*), GSH homeostasis, and redox balance (*Ggt1*, *Gstt1*, *Ugt2b5*) genes were also relatively suppressed in *Gsr*-KO embryonic lungs
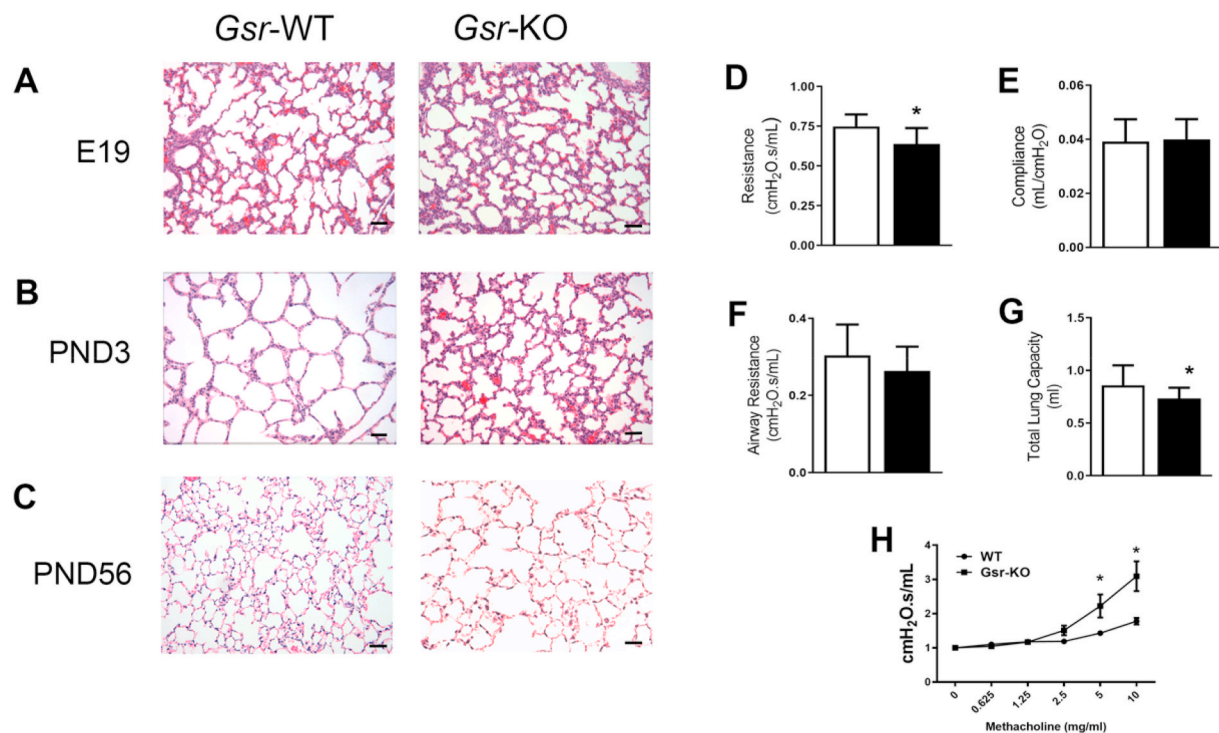
Fig. 2. Lung morphology of wild-type (*Gsr*-WT) and glutathione reductase-deficient (*Gsr*-KO) mouse lungs from canalicular to matured stages. H&E-stained lungs from *Gsr*-KO mice (200x) display evidence of septal thickening and alveolar epithelial dysplasia compared to *Gsr*-WT at embryonic day E19 (A) and persistent septal thickening alveolar epithelial cell dysplasia at PND3 (B) which has essentially normalized by PND56 (C). Bars = 50 μm. Pulmonary function assessment in PND56 mice for pulmonary resistance (D), compliance (E), total lung capacity (F) and airway resistance (G) were assessed. Pulmonary resistance and total lung capacity were significantly decreased in *Gsr*-KO mice compared to *Gsr*-WT. (H) Methacholine responses reveal enhanced airway responsiveness in *Gsr*-KO compared to *Gsr*-WT at PND 56. Data are expressed as mean +SEM (*$p < 0.05$ vs *Gsr*-WT; n=14–18).
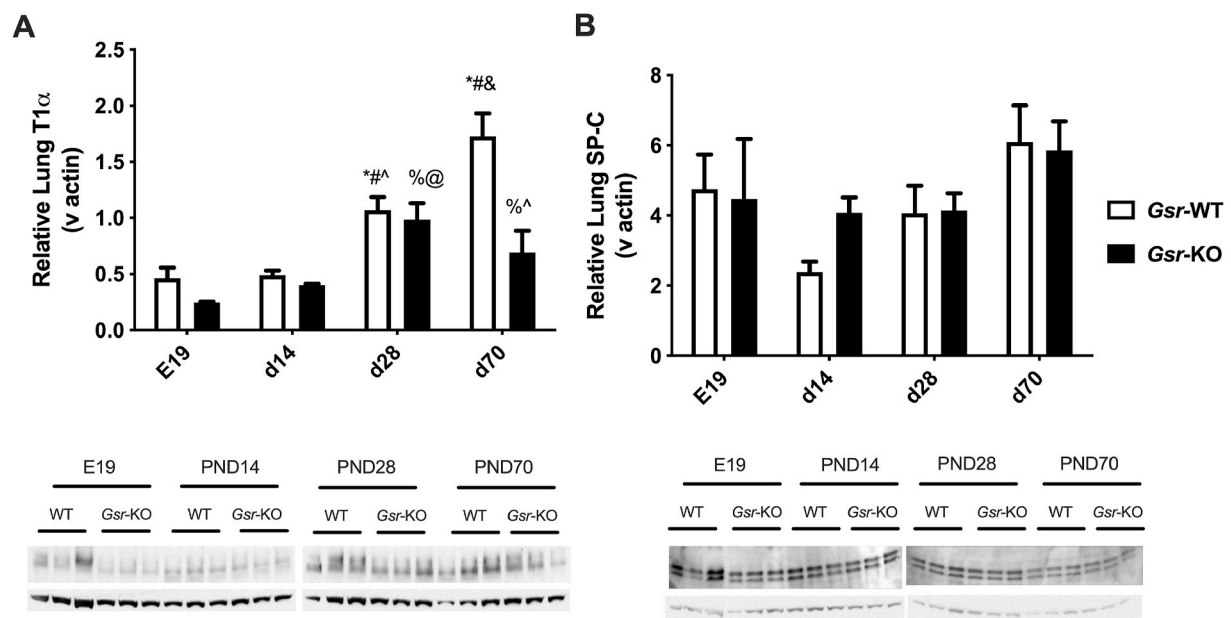

Fig. 3. Western Blot analyses for T1-alpha (T1α) and surfactant protein C (SP–C) in glutathione reductase-deficient (*Gsr*-KO) and -sufficient (*Gsr*-WT) mouse lungs. (A) Independent effects of genotype and day of life on lung T1α expression and an interaction between day of life and genotype were detected. (B) No effects or interactions were detected. Data are expressed as mean +SEM (n=3) and were assessed by two-way ANOVA followed by Newman-Keuls post hoc. $P < 0.05$ *vs E19-*Gsr*-WT, #vs PND14 *Gsr*-WT, &vs PND28-*Gsr*-WT, ^vs PND70-*Gsr*-WT, %vs E19-*Gsr*-KO, @vs PND14-*Gsr*-KO.

(Tables 1 and S1). *Gsr* deficiency may thus predispose the animals to altered pulmonary immune and inflammatory responses.

At the saccular to alveolar transition (PND5), *Gsr* deficiency significantly affected the expression of 448 transcripts ($p < 0.01$). Most predominantly, the transcripts involved in lipid metabolism and process (e.g., apolipoprotein family, albumin), coagulation system (e.g., fibrinogens, serine (or cysteine) peptidase inhibitor family), and acute phase responses (alpha-2-macroglobulin) were suppressed in *Gsr-KO* lungs
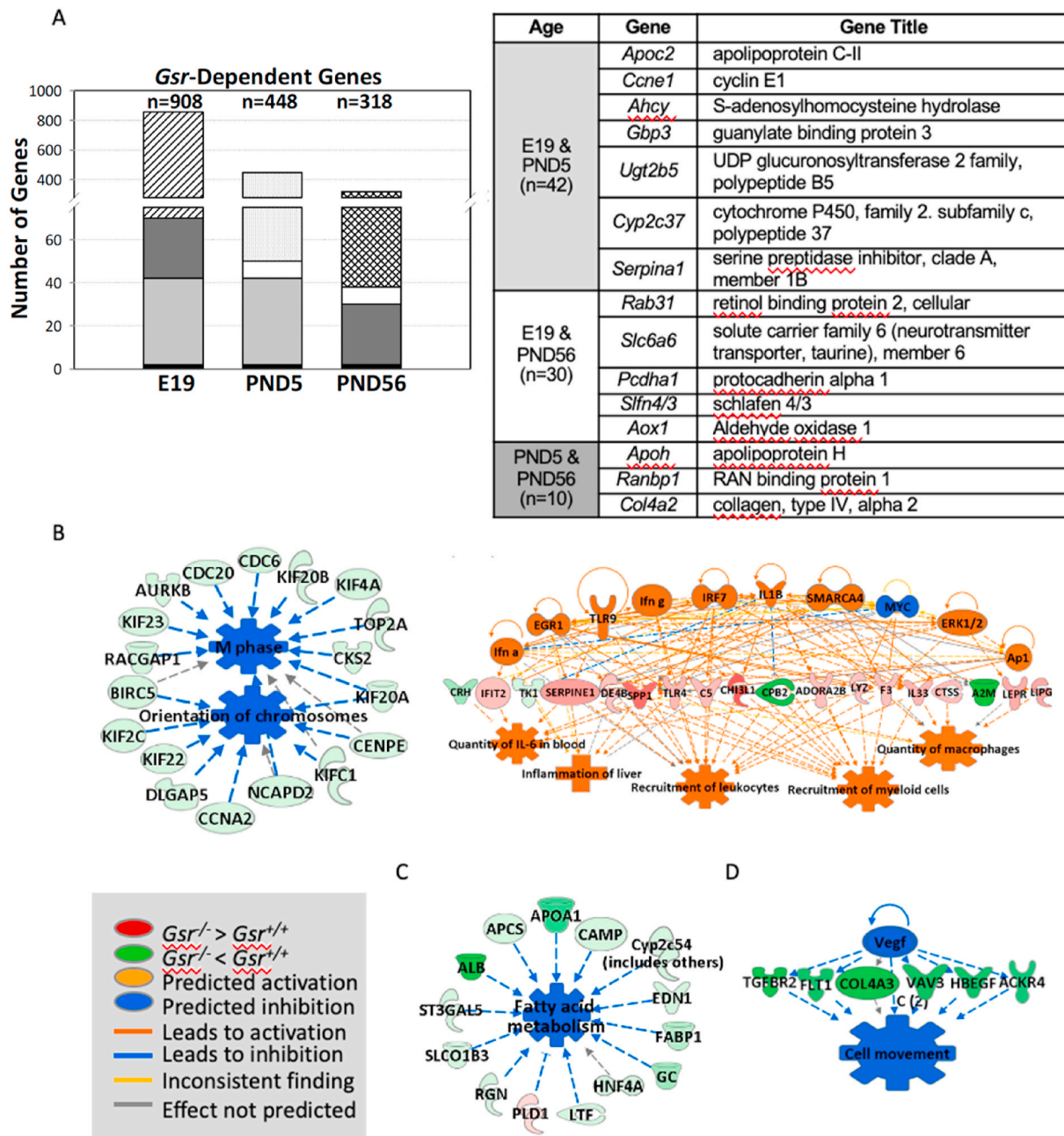
Fig. 4. Effect of glutathione reductase (*Gsr*) deficiency on embryonic and postnatal lung transcriptomics. (A) Venn Diagram analysis determined *Gsr*-dependently expressed genes at embryonic day E19 and postnatal days 5 (PND5) and PND56. Common *Gsr*-dependent genes at different developmental ages are shown as same color/pattern blocks in the bar graphs. (B) At E19 (canalicular stage), lungs in Gsr-deficient (*Gsr*-KO) embryo displayed significantly lowered expression of genes for cell cycle control of chromosomal replication and DNA damage checkpoint regulation and heightened expression of inflammatory and cell death response genes. (C) At PND5 (entering alveolar stage), *Gsr*-KO lungs showed significantly suppressed transcriptome for lipid metabolism and transport and coagulation system. (D) In mature lung (PND56), *Gsr* deficiency modulated genes to promote abnormal cardiovascular system function and connective tissue disorders. Analyses were done using GeneSpring (moderated *t*-test followed by Benjamini-Hochberg multiple testing correction, $p < 0.01$) and Ingenuity Pathway Analysis software. (For interpretation of the references to color in this figure legend, the reader is referred to the Web version of this article.)

versus *Gsr-WT* lungs (Fig. 4C, Tables 1 and S2). These data suggest that GSR is likely essential in surfactant production and other lipid-related lung developmental processes as well as blood coagulation during the saccular-to-alveolar transition stage. This may explain the histologic interruption of alveolar budding beginning at this stage in *Gsr-KO* lungs (Fig. 2B).

In the mature (PND56) lung, the effect of *Gsr* deficiency on the transcriptome was relatively marginal (n=318, $p < 0.01$). Genes differentially expressed between two genotypes (Tables 1 and S3) were mainly involved in connective tissue development, angiogenesis, and

cardiovascular function (Fig. 4D). Transcripts constitutively lower in *Gsr-KO* than in *Gsr-WT* at PND56 included collagens (e.g., collagen type IV), transforming growth factor, beta receptor II (*Tgfbr2*), neuron-derived neurotrophic factor (*Ndnf*), and vinculin (*Vcl*) (Tables 1 and S3).

3.5. Differential effects of neonatal hyperoxic exposure on Gsr-WT and Gsr-KO mice

Characteristic alveolar simplification was present in *Gsr*-WT/0.85 mice at PND14 (Fig. 5B) as evidenced by decreased alveolar number

Table 1
Representative glutathione reductase (*Gsr*)-dependent genes in embryo to adult mouse lungs.

Category (Age)	RefSeq ID	†FD	Gene Symbol	Gene Title	Functions
Cell cycle, DNA damage checkpoint regulation (E19)	NM_001025779	−3.14	*Cdc6*	cell division cycle 6	DNA replication initiation
	NM_007659	−2.26	*Cdk1*	cyclin-dependent kinase 1	protein complex assembly
	NM_001302540	−2.66	*Mcm5*	minichromosome maintenance deficient 5	DNA replication initiation
	NM_001291185	−2.41	*Aurka*	aurora kinase A	meiotic spindle organization
	NM_172301	−2.36	*Ccnb1*	cyclin B1	mitotic cell cycle
	NM_001195298	−2.24	*Kifc1*	kinesin family member C1	mitotic sister chromatid segregation
Redox and metabolism (E19)	NM_029562	−32.87	*Cyp2d26*	cytochrome P450, family 2, subfamily d, polypeptide 26	xenobiotic metabolic process
	NM_001039555	−25.90	*Cyp2c68*	cytochrome P450, family 2, subfamily c, polypeptide 68	xenobiotic metabolic process
	NM_019775	−19.54	*Cpb2*	carboxypeptidase B2 (plasma)	fibrinolysis
	NM_001304800	−18.34	*Hsd3b1*	hydroxy-delta-5-steroid dehydrogenase, 3 beta- and steroid delta-isomerase 1	lipid metabolism
	NM_001277944	−15.45	*Apoc2*	apolipoprotein C-II	lipid metabolism
	NM_009467	−12.76	*Ugt2b5*	UDP glucuronosyltransferase 2 family, polypeptide B5	phase 2 conjugation
	NM_001305992	−3.25	*Ggt1*	gamma-glutamyltransferase 1	glutamate metabolic process
	NM_008185	−2.88	*Gstt1*	glutathione S-transferase, theta 1	glutathione metabolic process
Inflammatory and immunological response (E19)	NM_009892	3.14	*Chil3*	chitinase-like 3	polysaccharide catabolic process
	NM_001164724	2.43	*Il33*	interleukin 33	leukocyte migration
	NM_133871	3.66	*Ifi44*	interferon-induced protein 44	immune response
	NM_008331	6.73	*Ifit1*	interferon-induced protein with tetratricopeptide repeats 1	immune system process, response to virus
	NM_001099217	4.35	*Ly6c1*	lymphocyte antigen 6 complex, locus C1	Activation of lymphocytes
	NM_022983	5.03	*Lpar3*	lysophosphatidic acid receptor 3	activation of MAPK activity
	NM_144559	2.51	*Fcgr4*	Fc receptor, IgG, low affinity IV	NK T cell proliferation
	NM_021297	2.42	*Tlr4*	toll-like receptor 4	innate immune response
	NM_016704	3.37	*C6*	complement component 6	in utero embryonic development
Coagulation system/Acute phase response signaling (PND5)	NM_175628	−8.24	*A2m*	alpha-2-macroglobulin	negative regulation of complement activation
	NM_009244	−21.46	*Serpina1b*	serine (or cysteine) preptidase inhibitor, clade A, member 1 B	protein N-linked glycosylation
	NM_001111048	−39.04	*Fga*	fibrinogen alpha chain	adaptive immune response
	NM_008407	−9.09	*Itih3*	inter-alpha trypsin inhibitor, heavy chain 3	peptidase inhibitor activity
	NM_017371	−4.13	*Hpx*	hemopexin	positive regulation of immunoglobulin production
	NM_031164	−6.00	*F13b*	coagulation factor XIII, beta subunit	blood coagulation pathway
	NM_013697	−23.5	*Ttr*	transthyretin	retinol metabolic process, thyroid hormone transport
Lipid metabolism (PND5)	NM_001277944	−4.54	*Apoc2*	apolipoprotein C-II	lipid transport
	NM_009692	−16.65	*Apoa1*	apolipoprotein A-I	lipid transporter activity
	NM_009654	−27.57	*Alb*	albumin	fatty acid binding, transport
	NM_007443	−8.44	*Ambp*	alpha 1 microglobulin	protein-chromophore linkage
Angiogenesis, connective tissue disorder (PND56)	NM_172399	−2.54	*Ndnf*	neuron-derived neurotrophic factor	angiogenesis
	NM_054077	−2.25	*Prelp*	proline arginine-rich end leucine-rich repeat	axonogenesis
	NM_007734	−1.87	*Col4a3*	collagen, type IV, alpha 3	negative regulation of angiogenesis
	NM_009371	−1.86	*Tgfbr2*	transforming growth factor, beta receptor II	patterning of blood vessels

†Fold difference of baseline lung gene expression between *Gsr*-WT and *Gsr*-KO mice at the designated age (negative values indicate lowered expression in *Gsr*-KO than in *Gsr*-WT, positive values indicate heightened expression in *Gsr*-KO than in *Gsr*-WT). Full lists of the significantly varied genes between two genotypes determined by moderated *t*-test ($p < 0.01$) are in Supplementary Tables S1–S3. E=embryonic day. PND=postnatal day.

(Fig. 5E) and increased alveolar perimeter (Fig. 5F). In *Gsr*-KO/0.21 mice at PND14, evidence of persistent alveolar epithelial dysplasia remained (Fig. 5C) and was quantitatively reflected by decreased alveolar number (Fig. 5E). Morphometric analyses indicated independent effects of and an interaction between hyperoxia and genotype on alveolar number and perimeter (Fig. 5E and F). The effects of hyperoxia on lung architecture in *Gsr*-WT mice were comparatively blunted in *Gsr*-KO mice (Fig. 5E and F).

3.6. Compensatory effects within the TXN system in Gsr-KO mice with and without oxygen exposure

By PND7 in *Gsr*-WT animals, the effects of hyperoxia on the pulmonary TXN system are variable with no change in TXN1, but increase in *TXN2* expression, and a trend toward an increase in TXNRD1 (Fig. 6). In contrast, *Gsr* deficiency altered the baseline expression of the TXN system with increased TXN1 and TXN2 expression. Exposure to hyperoxia potentiated this effect relative to *Gsr*-KO/0.21, as well as both *Gsr*-

WT/0.21 and *Gsr*-WT/0.85 mice (Fig. 6A, C). Similarly, TXNRD1 expression was significantly upregulated in *Gsr*-KO/0.85 mice when compared to all other groups (*Gsr*-KO/0.21, *Gsr*-WT/0.21 and *Gsr*-WT/0.85), although not significantly increased at baseline in *Gsr*-KO/0.21 compared to *Gsr*-WT/0.21 mice (Fig. 6B). Western blot analysis indicated an effect of genotype and exposure on the expression of TXN1, TXN2 and TXNRD1, as well as an interaction for TXNRD1 and TXN2 expression based on genotype and exposure.

3.7. Effect of neonatal hyperoxic exposure on lung transcriptomics

At the saccular to alveolar transition (PND5), hyperoxic exposure alone caused 1129 genes to be differentially expressed in *Gsr*-WT mice, whereas *Gsr* deficiency modulated these changes to only 663 genes (Fig. 7A). A total of 303 transcripts were significantly ($p < 0.01$) modulated by hyperoxia in a *Gsr*-dependent manner (Table 2 and S4). Interestingly, many of these genes were basally suppressed in *Gsr*-KO neonates relative to *Gsr*-WT neonates while they were upregulated by
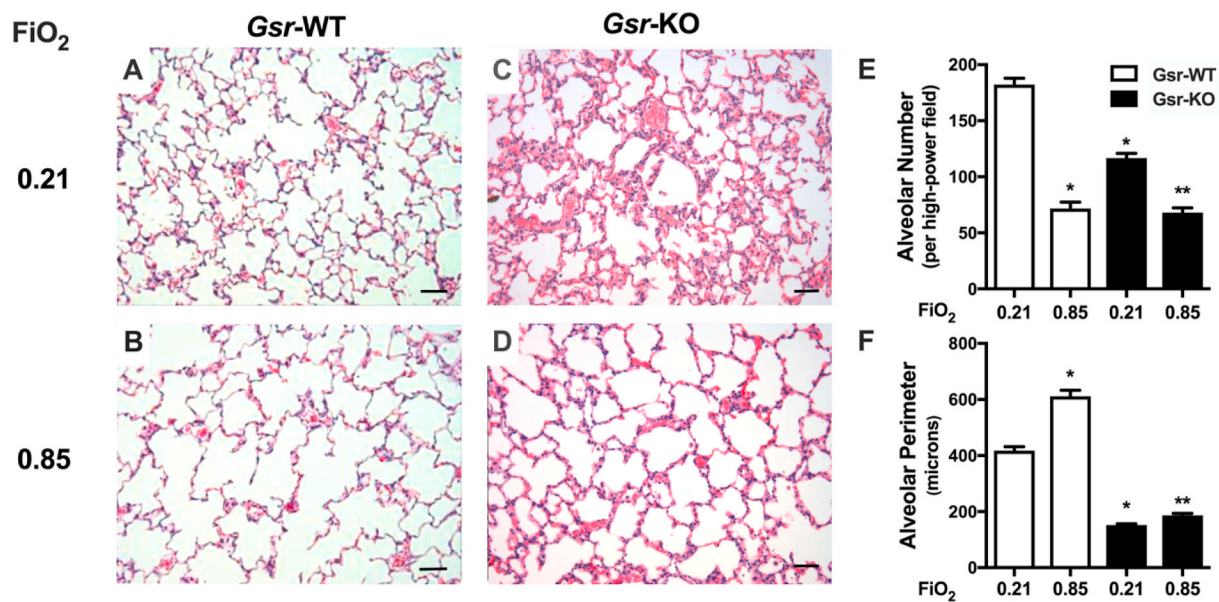
Fig. 5. Effects of neonatal hyperoxic exposure on glutathione reductase-sufficient (*Gsr*-WT) and -deficient (*Gsr*-KO) mice. (A) H&E-stained lung sections (200x) from PND14 *Gsr*-WT and *Gsr*-KO neonates exposed to room air (FiO$_2$ 0.21) or hyperoxia (FiO$_2$ 0.85) for 14 d (PND0-14). Characteristic alveolar simplification is present in hyperoxia-exposed *Gsr*-WT mice while evidence of persistent alveolar epithelial dysplasia remains in *Gsr*-KO mice after hyperoxia exposure. (B) Independent effects of and an interaction between hyperoxia and genotype on alveolar number and perimeter. Data are expressed as mean +SEM (n=3–5). *$p < 0.05$ vs *Gsr*-WT/Room Air. **$p < 0.05$ vs *Gsr*-KO/Room Air. Bars = 50 μm.
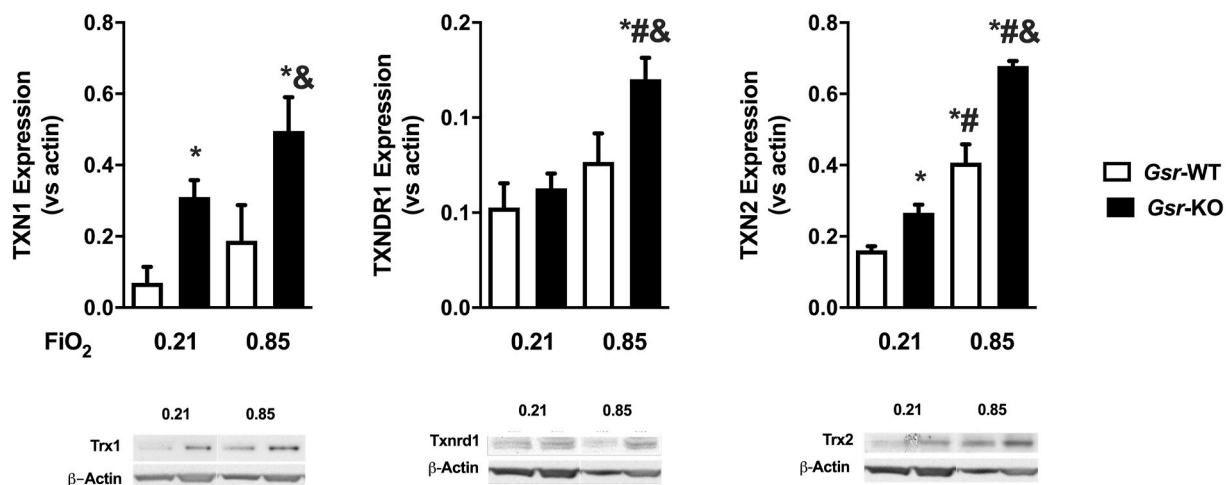

Fig. 6. Effects of glutathione reductase (Gsr) deficiency and hyperoxia on the pulmonary thioredoxin (TXN) system at PND7. Protein levels of TXN1, TXN reductase 1 (Txnrd1), and TXN2 normalized by actin levels in wild-type (*Gsr*-WT) and *Gsr*-deficient (*Gsr*-KO) neonatal mice. 2-Way ANOVA followed by Tukey's post hoc revealed an effect of genotype and exposure on the expression of all three proteins, as well as an interaction on TXNRD1 and TXN2 expression. Data expressed as mean +SEM (n=3), $p < 0.05$ *vs *Gsr*-WT/0.21, #vs *Gsr*-KO/0.21, &vs *Gsr*-WT/0.85.

hyperoxia only in *Gsr*-KO mice as depicted in the heat map from hierarchical clustering analysis (Fig. 7A). Venn diagram analysis determined that only 96 common genes were modulated by hyperoxia in both genotypes (Fig. 7A, Tables S5 and S6). The *Gsr*-dependent, hyperoxia-responsive genes included multiple keratins, myosins, actins, and calcium channels (Fig. 7B, Tables 2 and S4), which were highly associated with abnormal cytoskeleton and skeletal-muscular function and tissue morphology (Fig. 7C). On the other hand, these genes were also predicted to inhibit respiratory failure and neonatal death through activation of upstream myogenic differentiation 1 (MYOD1) and β-catenin (CTNNB1) in hyperoxia-exposed *Gsr*-KO neonates (Fig. 7D). There was marked upregulation of genes involved in neuronal nitric oxide synthase signaling (e.g., *Cacng1, Nos1, Ryr1*), calcium signaling (*Acta1, Caso1, Myh, Tnnc2*), and glycolysis/ketolysis (e.g., *Fbp2, Eno3, Pfkm, Bdh1,*

Acat1) as well as keratins and myosins (Table S6), in the neonate hyperoxia-exposed *Gsr*-KO lungs. These transcriptome changes suggeste that compromise of the morphology and function in connective tissue and muscle may explain the morphologic features of *Gsr*-KO neonates after hyperoxia exposure (Fig. 5).

At 8 weeks of age, 6 weeks after termination of hyperoxic exposure, 403 genes ($p < 0.01$) were significantly different between neonatal hyperoxia-exposed and neonatal air exposed *Gsr*-WT mice (Table S7). Chemokine and other inflammatory genes (e.g., *Cxcl5, Cxcl3, Ccl17, Mmp12*) were a distinguished cluster of genes that were more abundantly expressed in neonatal hyperoxia-exposed lungs than in air-exposed lungs with prediction of activated upstream regulators including tumor necrosis factor and nuclear factor-kappa B (Supplementary Fig. S2A). Dysregulation of tissue and vessel development and
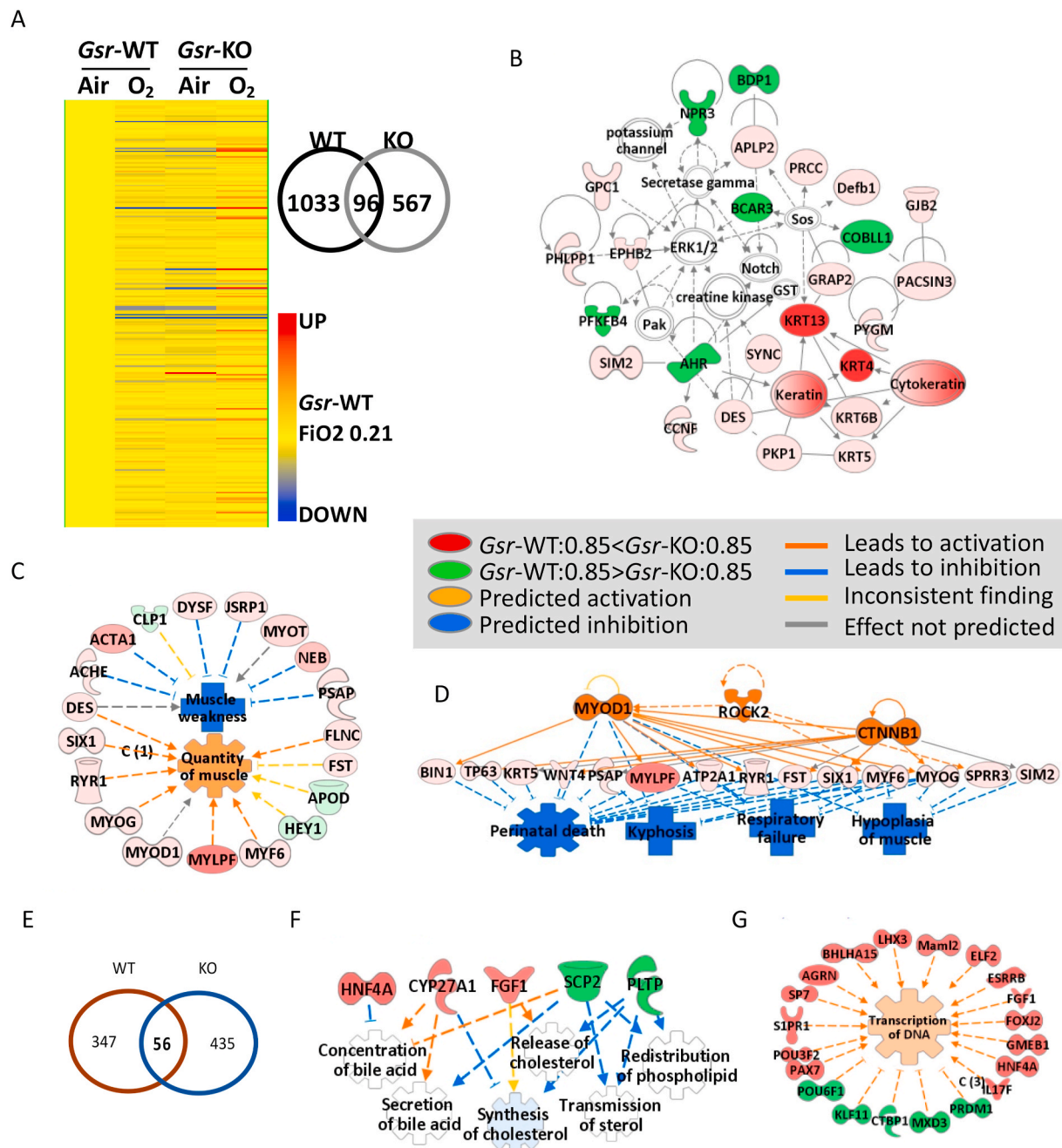
Fig. 7. Effects of glutathione reductase (Gsr) deficiency and hyperoxia (85% O_2) on lung transcriptomics. (A) Heat map from hierarchical clustering analysis depicts lung expression profiles of Gsr-dependently hyperoxia (0.85 FiO_2)-responded genes at postnatal day 5 (PND5) after hyperoxia exposure (PND0-PND5, n = 303, 2-way ANOVA with $p < 0.01$). Color bar indicates average expression intensity (n = 3/group) normalized to wild-type (*Gsr*-WT)-Air (0.21 FiO_2) group. Venn Diagram analysis depicted number of genotype-specific hyperoxia responsive genes determined by moderated *t*-test in *Gsr*-WT and Gsr-deficient (*Gsr*-KO) neonates. (B) Hyperoxia altered lung genes involved predominantly in cytoskeleton and skeletal/muscular development and tissue and cell morphology in *Gsr*-KO neonates. (C) The key molecular network of the Gsr-dependently altered neonatal lung genes by hyperoxia was cytoskeleton and skeletal-muscular function and tissue morphology and development. (D) Hyperoxia-altered genes in *Gsr*-KO neonates may inhibit respiratory failure and neonatal death through activation of upstream molecules such as myogenic differentiation 1 (Myod1) and β-catenin (CTNNB1). (E) Venn Diagram analysis depicted number of genotype-specific hyperoxia responsive genes following recovery from neonatal hyperoxia recovery within *Gsr*-WT and *Gsr*-KO adult mice. (F) Neonatally exposed hyperoxia was predicted to inhibit genes involved in lipid metabolism (e.g., bile acid, cholesterol) and enhance genes involved in transcription of adulthood lungs in *Gsr*-KO mice. Analysis was done by GeneSpring and Ingenuity Pathway Analysis software. Molecules colored by expression levels of *Gsr*-KO/0.85 FiO_2 at PND5 (vs *Gsr*-WT/0.85 FiO_2). (For interpretation of the references to color in this figure legend, the reader is referred to the Web version of this article.)

increased mortality and lymphocytic tumorigenesis were also identified by pathway analysis (Supplementary Figs. S2–B). These data indicate that ongoing adverse pulmonary molecular events into adulthood may adversely influence the persistent BPD-like phenotype. Between *Gsr*-WT and *Gsr*-KO mice, 491 lung genes were significantly varied ($p < 0.01$) at

PND56 and after neonatal exposure although expression difference of these genes were marginal (<2-folds, Table 3 and S8). Of the 491 genes differentially expressed between the genotypes at PND56 following oxygen exposure, 56 genes were similarly altered by oxygen exposure in the *Gsr*-WT animals leaving 435 genes that were uniquely altered by Gsr

Table 2
Representative glutathione reductase (*Gsr*)-dependent neonate lung genes regulated by hyperoxia exposed during postnatal days (PND0-PND5).

RefSeq ID	p	[a]FC WT	[a]FC KO	¶FD	Gene Symbol	Gene Title
NM_001313949	0.001502453	−5.40	34.61	36.03	*Krt13*	keratin 13
NM_008475	7.66E-04	−4.69	20.55	21.29	*Krt4*	keratin 4
NM_177369	0.0081382	−1.69	48.45	19.19	*Myh8*	myosin, heavy polypeptide 8, skeletal muscle, perinatal
NM_027416	0.001268343	−2.70	7.90	9.26	*Calml3*	calmodulin-like 3
NM_001272041	0.005731548	−1.50	21.62	7.56	*Acta1*	actin, alpha 1, skeletal muscle
NM_001081123	3.51E-04	−1.34	8.05	5.92	*Arhgap36*	Rho GTPase activating protein 36
NM_028798	0.001839206	−2.15	4.21	5.20	*Crct1*	cysteine-rich C-terminal 1
NM_028216	0.008994052	−2.29	4.52	4.92	*Psca*	prostate stem cell antigen
NM_001101605	0.0049872	−1.91	4.34	4.90	*Ifit1bl1*	interferon induced protein with tetratricpeptide repeats 1 B like 1
NM_013456	0.006323175	−1.12	6.94	4.67	*Actn3*	actinin alpha 3
NM_001164787	0.007458202	−2.65	4.38	4.64	*Sprr2a1, etc.*	small proline-rich protein 2A1, etc.
NM_001033239	0.002655688	−1.90	5.58	4.51	*Csta1*	cystatin A1
NM_173385	0.0084611	−1.54	3.61	4.50	*Cilp*	cartilage intermediate layer protein, nucleotide pyrophosphohydrolase
NM_007582	0.001477798	−1.80	3.55	4.22	*Dsc2*	desmocollin 2
NM_013505	0.001027153	−1.15	4.35	4.05	*Cacng1*	calcium channel, voltage-dependent, gamma subunit 1
NM_008657	0.008563787	−1.37	3.87	3.54	*Myf6*	myogenic factor 6
NM_001081375	0.003077287	−1.92	3.02	3.29	*Cnfn*	cornifelin
NM_001081157	0.004109589	−1.44	2.83	3.27	*Lmod3*	leiomodin 3 (fetal)
NM_001033131	0.0016160	−1.41	2.92	3.17	*Krtdap*	keratinocyte differentiation associated protein
NM_009109	0.004861059	−1.15	3.82	3.12	*Ryr1*	ryanodine receptor 1, skeletal muscle
NM_007812	0.0023872	−1.31	3.12	2.90	*Cyp2a4*	cytochrome P450, family 2, subfamily a, polypeptide 4
NM_007376	0.004647014	−9.79	−1.18	−1.59	*Pzp*	pregnancy zone protein
NM_008725	0.008516206	1.42	−19.17	−1.52	*Nppa*	natriuretic peptide type A
NM_001012766	0.0036717	1.20	−1.30	−1.36	*Ear1*	eosinophil-associated, ribonuclease A family, member 1
NM_007707	0.006182605	1.41	−1.01	−1.32	*Socs3*	suppressor of cytokine signaling 3
NM_001150749	0.007889654	−5.05	1.04	−1.32	*Rdh7*	retinol dehydrogenase 7
NM_030110	0.0063489	1.27	−1.01	−1.27	*Micu3*	mitochondrial calcium uptake family, member 3

¶Fold difference of gene expression between *Gsr*-WT and *Gsr*-KO mice at the end of 5-day hyperoxia exposure at PND5 (negative values indicate lower expression in *Gsr*-KO than in *Gsr*-WT, positive values indicate higher expression in *Gsr*-KO than in *Gsr*-WT). Full lists of the *Gsr*-dependently varied neonatal lung genes by hyperoxia ($n=303$, 2-way ANOVA $p < 0.01$) are in Supplementary Table S4.

[a] Fold change after 5-day hyperoxia exposure in *Gsr*-WT or in *Gsr*-KO over genotype-matched air-exposed controls (negative values indicate decreased expression by hyperoxia, positive values indicate increased expression by hyperoxia).

Table 3
Representative glutathione reductase (*Gsr*)-dependent lung genes at postnatal day 56 (PND56) after neonatal hyperoxia exposure.

RefSeq ID	p	[a]FC WT	[a]FC KO	¶FD	Gene Symbol	Gene Title
NM_001177713	0.00457	−1.73	2.26	4.13	*Cyp26b1*	cytochrome P450, family 26, subfamily b, polypeptide 1
NM_001166627	0.001644	−1.30	1.03	1.49	*Dynlt1-ps1*	dynein light chain Tctex-type 1, pseudogene 1///dynein light chain Tctex-type 1A
NM_010731	4.38E-04	−1.91	1.12	1.49	*Zbtb7a*	zinc finger and BTB domain containing 7a
NM_144879	5.83E-04	−1.21	1.30	1.42	*Vash2*	vasohibin 2
NM_146244	4.96E-05	−1.15	1.32	1.36	*Rps6kl1*	ribosomal protein S6 kinase-like 1
NM_022033	0.004434	−1.30	1.22	1.35	*Oxct2a*	3-oxoacid CoA transferase 2A
NM_203320	0.005966	5.21	1.32	−1.81	*Cxcl3*	chemokine (C-X-C motif) ligand 3
NM_010861	0.005792	1.09	−3.33	−1.76	*Myl2*	myosin, light polypeptide 2, regulatory, cardiac, slow
NM_010780	6.16E-04	1.36	−1.15	−1.47	*Cma1*	chymase 1, mast cell
XM_006504243	0.00933	1.42	−1.26	−1.47	*Tmem156*	transmembrane protein 156
NM_019514	6.26E-04	1.35	−1.16	−1.43	*Astn2*	astrotactin 2
NM_201638	0.002129	1.18	−1.41	−1.40	*Mettl14*	methyltransferase like 14
NM_009140	0.003614	2.65	1.24	−1.27	*Cxcl2*	chemokine (C-X-C motif) ligand 2
NM_019810	0.006028	1.88	1.23	−1.36	*Slc5a1*	solute carrier family 5 (sodium/glucose cotransporter), member 1
NM_009100	0.008386	1.59	−1.09	−1.35	*Rptn*	repetin
NM_001099774	0.008755	1.08	−1.63	−1.13	*Krtap17-1*	keratin associated protein 17-1
NM_009162	3.89E-06	1.18	−1.48	−1.12	*Scg5*	secretogranin V

¶Fold difference of lung gene expression between *Gsr*-WT and *Gsr*-KO mice at PND56 after neonatal hyperoxia exposure (negative values indicate lower expression in hyperoxia-PND56 *Gsr*-KO than in hyperoxia-PND56 *Gsr*-WT, positive values indicate higher expression in hyperoxia-PND56 *Gsr*-KO than in hyperoxia-PND56 *Gsr*-WT). Full lists of the *Gsr*-dependently varied lung genes during recovery after neonate hyperoxia exposure ($n=491$, 2-way ANOVA $p < 0.01$) are in Supplementary Table S8.

[a] Fold change in PND56 lung after neonate-hyperoxia exposure compared to neonate-air exposure in each genotype (negative values indicate decreased expression in neonate hyperoxia-exposed lung than in neonate air-exposed lung, positive values indicate increased expression in neonate hyperoxia-exposed lung than in neonate air-exposed lung).

deficiency (Fig. 7E). Interestingly, up or downregulation trends of many genes were opposite in *Gsr*-WT and *Gsr*-KO mice at this time point (Tables 3 and S8). Pathway analysis demonstrated that lack of *Gsr* may drive transcriptome changes in nerve and tissue development and morphology, cell-to-cell signaling, RNA transcription, and lipid metabolism (e.g., bile acid, cholesterol) in adulthood lungs exposed to neonatal hyperoxia (Fig. 7F).

4. Discussion

The effect of *Gsr* deficiency in the neonatal period has not been previously described. We quantified (compared) lung GSH, GSSG and GSH/GSSG levels in 6-week old adult *Gsr*-WT and *Gsr*-KO mice and found an increase in GSSG levels and a dramatic decrease in the GSH/GSSG ratio in *Gsr*-KO mice [8]. In contrast, our current neonatal studies show a significant decrease in all components in the glutathione redox

cycle suggesting that the increased GSSG levels detected in adult animals build up over time as the animal is unable to reduce GSSG to GSH in order to recycle reducing equivalents. Neonatal mammals are known to have immature redox systems which place them at risk for oxidative stress and damage, especially when born prematurely or exposed to postnatal stressors [23–27].

The GSH and GSSG deficits within our *Gsr*-KO mice reveal an inability to stimulate this intracellular antioxidant system in the neonatal period as was observed in the *Gsr*-WT mice. Our data also suggest a progressive decline in redox potential in Gsr-KO mice as evidenced by the decreasing GSH:GSSG Eh during the neonatal period. GSH + GSSG levels were lower in *Gsr*-KO mice though the mechanism for this finding is not entirely clear. A review of transcriptomic data revealed no strain-dependent differences in the expression of genes required for *de novo* GSH synthesis, including glutamate-cysteine ligase, glutamate-cysteine ligase catalytic subunit, and glutathione synthetase. It is possible that the cysteine pool is lower in *Gsr*-KO mice when compared to wild-type mice, though these investigations are beyond the scope of the present study.

Our previous experience with *Gsr*-KO mice indicated that no lung phenotype was present in adulthood [6,8]. We first investigated the maturation of the lung during the late canalicular and late saccular phases of murine lung development. These stages of lung development are prior to alveolarization, when standard, objective morphometric quantification is valid [28]; Gross examination of canalicular phase lungs at E19 revealed the presence of septal thickening and epithelial dysplasia. Similar epithelial abnormalities persisted into the saccular phase at PND3 with thickened septal walls and disorganization of the developing saccules. In the absence of formal morphometric analyses at the canalicular and saccular phase of lung development, lung samples were assessed by a murine pathologist who found the *Gsr*-KO lungs to be significantly different than WT controls with the presence of epithelial cell dysplasia and decreased transdifferentiation of AT2 to AT1 cells. With the onset of the alveolar lung development, there is the exponential expansion of the alveoli due to transdifferentiation of AT2 to AT1 cells which is represented in the doubling of the lung weight and alveoli numbers between PND5 and 7 [29–32]. By examining AT2 and AT1 cell markers *via* Western blot at this time point, our data supported deficits in the ability of AT2 cells to transdifferentiate into AT1 cells as described by the pathologist. By PND14, there were still abnormalities of the alveolar architecture when quantified by formal morphometric analyses. *Gsr*-KO mice exhibited a more homogeneous lung phenotype as there were less complete alveoli per high power field and those that could be quantified had a smaller perimeter. Usually, these two morphology parameters track together with decreased numbers correlating with significantly enlarged airway perimeters. We speculate that the *Gsr*-KO animals have many enlarged air-sacs that could not be counted due to the field of view of the microscope.

In accordance with our previous experience, the lung architecture was relatively normal by adulthood in *Gsr*-KO mice. Looks can be deceiving, however, as functional assessments identified pulmonary function deficits and airway hypersensitivity that had not previously been appreciated. Physiologically, airway resistance comes from tethering of the lung parenchyma by alveolar segments. Thus, decreased resistance in for *Gsr*-KO mice might reflect subtle alveolar abnormalities not appreciated under gross structural examination [33] or decreases in matrix deposition that affect lung structure itself. Similarly, increased sensitivity to methacholine indicates an airway hyperactivity to stimuli similar to that seen in childhood for patients with a history of BPD and in other models with altered reactive oxygen species [34–37].

To determine potential mechanisms driving structural abnormalities in *Gsr*-KO lungs, we next investigated the effects of Gsr-deficiency on gene expression and cell signaling pathways. Whole lung transcriptome analysis identified differentially expressed genes over time due to aging between the genotypes. Consistent with the pronounced histopathologic differences between *Gsr*-WT and *Gsr*-KO at earlier timepoints, the most dramatic transcriptomic changes were present in the embryonic tissues during the canalicular phase of lung development. The differences decreased by almost half with the transition to the late saccular stage at PND5. Similar to our histopathologic findings, the transcriptomic phenotype was less distinct between the genotypes in adulthood.

Genes with differential expression in Gsr-deficiency were not static throughout lung development and our data revealed unique sets of genes and differential expression at embryonic and neonatal timepoints. Decreased expression of genes related to cell cycle pathways and cell division at E19 are plausible explanations for the histopathologically dysplastic epithelium present at these early timepoints. At PND5, the *Gsr*-KO mouse lung transcriptome was reflective of impaired lipid metabolism and surfactant production preceding the beginning of alveolarization. Lipid metabolism, including specifically surfactant production, is a highly oxidative process that occurs within the endoplasmic reticulum [38,39]. The glutathione redox potential within the endoplasmic reticulum depends in GSH import [40]. Given our finding of decreased intracellular GSH levels in the *Gsr*-KO animals, we speculate that there is decreased reducing equivalents to buffer these processes within the ER. Surfactant production is mediated by AT2 cells. In the rodent, surfactant production begins in the canalicular phase and increases through the saccular alveolar stage [32,38]. Though our data suggests that the total quantity of AT2 cells is not affected by *Gsr* deficiency, the AT2 cell function may be compromised. Poor *Gsr*-KO AT2 function is supported by the finding of decreased transdifferentiation into AT1 cells and the transcriptomic changes in surfactant production. The compensatory increase of TXN to maintain intracellular redox balance may not be effective within the endoplasmic reticulum or even be transported into the endoplasmic reticulum, and therefore, unable to compensate for oxidative stress during lipid transport. By adulthood, the pathways that remained active in the *Gsr*-KO animals were less connected to the pulmonary epithelium and more related to angiogenesis and cardiovascular function. Interestingly, fibrotic genes, such as collagens and *Tgfbr2* traditionally associated with hyperoxic lung injury models and BPD were significantly decreased in the *Gsr*-KO adult mice at baseline; changes in expression of these genes might contribute to the resistance towards hyperoxic lung injury previously reported in this genotype as adults [8,20,41,42].

As previously seen in our adult *Gsr*-KO studies, neonatal *Gsr*-KO mice had a blunted injury response to hyperoxia. Although the *Gsr*-KO mice had an abnormal baseline lung structure on morphometric analysis (as discussed above), the relative change between unexposed and oxygen exposed groups was comparatively less than in *Gsr*-WT animals. Following oxygen exposure, our data indicate an upregulation of the TXN system in *Gsr*-KO mice. It is likely that this compensatory response contributes to relative hyperoxic insensitivity to lung injury; however, such studies are beyond the scope of the present manuscript.

Similar to previous reports [21,43–45], we found a high number of genes to be differentially expressed following oxygen exposure in wild type animals. Conversely, this response was blunted in *Gsr*-KO mice and the directionality of the change in gene expression was inconsistent. Activation of pathways like myogenic differentiation and β-catenin in the *Gsr*-KO animals may contribute the blunted response to hyperoxia. Alterations in neuronal nitric oxide synthase signaling, glycolysis/ketolysis and keratins are predicted to coalesce into pathways that compromise morphology and structure of connective tissue which may explain the functional abnormalities that were present in the lungs.

Other groups have examined differential gene expression following recovery from neonatal hyperoxia exposure and found a similar decline in the number of differentially expressed genes [46]. As expected, in *Gsr*-WT animals we found persistent signals consistent with BPD-like phenotypes, such as dysregulation of tissue and vessel development and inflammation. Activation of tumor necrosis factor and nuclear factor-kappa B have been extensively described in murine models for BPD [47,48]. Interestingly, there was not a significant overlap of the differentially expressed genes between the genotypes after recovery

from hyperoxia exposure. Although *Gsr* deficiency may disrupt cell-to-cell signaling or lipid metabolism in adult lungs of mice exposed to hyperoxia during the neonatal period, there does not appear to be a persistent inflammatory or vascular phenotype.

The current studies support our initial hypothesis that GSR expression is necessary for normal perinatal lung maturation and development. Differences in lung redox status in *Gsr*-KO mice are evident shortly after birth and likely contribute to altered lung development, airway reactivity, and differential gene expression profiles. Furthermore, *Gsr*-deficient mice are less sensitive to the effects of hyperoxia, likely *via* compensatory upregulation of TXN-dependent cytoprotective responses as was similarly observed in adult mice. Our data reveal that alterations in GSH system functionality may drive epithelial dysregulation and altered lung development in the neonatal lung. Strategies that enhance GSH-dependent redox responses, such as TXN system modulation, may attenuate oxidative injury in the neonatal lung and reduce the incidence of BPD.

Author contributions

TET designed and supervised the study. MER, JMM, JRL, MLL, and MV conducted experiments. HYC and SRK performed microarray and bioinformatic analysis. TET, MER, LKR, and HYC wrote the manuscript.

Conflicts of interest

The authors declare that they have no conflict of interest.

Declaration of competing interest

The authors declare that they have no known competing financial interests or personal relationships that could have appeared to influence the work reported in this paper.

Acknowledgements

Appendix A. Supplementary data

Supplementary data to this article can be found online at https://doi.org/10.1016/j.redox.2020.101797.

References

[1] J.D. Crapo, Morphologic changes in pulmonary oxygen toxicity, Annu. Rev. Physiol. 48 (1986) 721–731. PubMed PMID: 3518622.

[2] R. Barrios, Z.Z. Shi, S.V. Kala, A.L. Wiseman, S.E. Welty, G. Kala, A.A. Bahler, C. N. Ou, M.W. Lieberman, Oxygen-induced pulmonary injury in gamma-glutamyl transpeptidase-deficient mice, Lung 179 (5) (2001) 319–330. PubMed PMID: 11976899.

[3] J. Nordberg, E.S. Arner, Reactive oxygen species, antioxidants, and the mammalian thioredoxin system, Free Radic. Biol. Med. 31 (11) (2001) 1287–1312. PubMed PMID: 11728801.

[4] S. Eriksson, J.R. Prigge, E.A. Talago, E.S. Arner, E.E. Schmidt, Dietary methionine can sustain cytosolic redox homeostasis in the mouse liver, Epub 2015/03/21, Nat. Commun. 6 (2015) 6479, https://doi.org/10.1038/ncomms7479. PubMed PMID: 25790857; PMCID: PMC4369796.

[5] S.V. Iverson, S. Eriksson, J. Xu, J.R. Prigge, E.A. Talago, T.A. Meade, E.S. Meade, M.R. Capecchi, E.S. Arner, E.E. Schmidt, A Txnrd1-dependent metabolic switch alters hepatic lipogenesis, glycogen storage, and detoxification, Epub 2013/06/08, Free Radic. Biol. Med. (2013), https://doi.org/10.1016/j.freeradbiomed.2013.05.028. PubMed PMID: 23743293.

[6] L.K. Rogers, T. Tamura, B.J. Rogers, S.E. Welty, T.N. Hansen, C.V. Smith, Analyses of glutathione reductase hypomorphic mice indicate a genetic knockout, Toxicol. Sci. 82 (2) (2004) 367–373. PubMed PMID: 15342956.

[7] R.H. Schirmer, R.L. Krauth-Siegel, G.E. Schulz, Coenzymes and cofactors, in: D. Dolphin, R. Poulson, O. Avramovic (Eds.), Coenzymes and Cofactors, John Wiley & Sons, Inc, New York, 1989, pp. 553–596.

[8] T.E. Tipple, S.E. Welty, L.K. Rogers, T.N. Hansen, Y.E. Choi, J.P. Kehrer, C. V. Smith, Thioredoxin-related mechanisms in hyperoxic lung injury in mice, Am. J. Respir. Cell Mol. Biol. 37 (4) (2007) 405–413. Epub 2007/06/19. doi: 2006-0376OC [pii] 10.1165/rcmb.2006-0376OC. PubMed PMID: 17575077; PMCID: 2176120.

[9] C.H. Williams, in: F. Muller (Ed.), Chemistry and Biochemistry of Flavoenzymes, CRC Press, Inc, Boca Raton, FL, 1992, pp. 121–211.

[10] R.D. Britt Jr., M. Velten, M.L. Locy, L.K. Rogers, T.E. Tipple, The thioredoxin reductase-1 inhibitor aurothioglucose attenuates lung injury and improves survival in a murine model of acute respiratory distress syndrome, Antioxidants Redox Signal. 20 (17) (2014) 2681–2691, https://doi.org/10.1089/ars.2013.5332. PubMed PMID: 24295151; PMCID: 4026403.

[11] K. Dunigan, Q. Li, R. Li, M.L. Locy, S.B. Wall, T.E. Tipple, The thioredoxin reductase inhibitor auranofin induces heme oxygenase-1 in lung epithelial cells via nrf2-dependent mechanisms, Epub 2018/07/20, Am. J. Physiol. Lung Cell Mol. Physiol. (2018), https://doi.org/10.1152/ajplung.00214.2018. PubMed PMID: 30024305.

[12] Q. Li, R. Li, S.B. Wall, K. Dunigan, C. Ren, T. Jilling, L.K. Rogers, T.E. Tipple, Aurothioglucose does not improve alveolarization or elicit sustained Nrf2 activation in C57BL/6 models of bronchopulmonary dysplasia, Epub 2018/01/26, Am. J. Physiol. Lung Cell Mol. Physiol. 314 (5) (2018) L736–L742, https://doi.org/10.1152/ajplung.00539.2017. PubMed PMID: 29368550; PMCID: PMC6008122.

[13] Q. Li, S.B. Wall, C. Ren, M. Velten, C.L. Hill, M.L. Locy, L.K. Rogers, T.E. Tipple, Thioredoxin reductase inhibition attenuates neonatal hyperoxic lung injury and enhances Nrf2 activation, Am. J. Respir. Cell Mol. Biol. (2016), https://doi.org/10.1165/rcmb.2015-0228OC. PubMed PMID: 27089175.

[14] M.L. Locy, L.K. Rogers, J.R. Prigge, E.E. Schmidt, E.S. Arner, T.E. Tipple, Thioredoxin reductase inhibition elicits nrf2-mediated responses in Clara cells: implications for oxidant-induced lung injury, Epub 2012/05/23, Antioxidants Redox Signal. (2012), https://doi.org/10.1089/ars.2011.4377. PubMed PMID: 22607006.

[15] R. Tindell, S.B. Wall, Q. Li, R. Li, K. Dunigan, R. Wood, T.E. Tipple, Selenium supplementation of lung epithelial cells enhances nuclear factor E2-related factor 2 (Nrf2) activation following thioredoxin reductase inhibition, Epub 2018/09/14, Redox Biol 19 (2018) 331–338, https://doi.org/10.1016/j.redox.2018.07.020. PubMed PMID: 30212802; PMCID: PMC6134185.

[16] W. Pretsch, Glutathione reductase activity deficiency in homozygous Gr1a1Neu mice does not cause haemolytic anaemia, Genet. Res. 73 (1) (1999) 1–5. PubMed PMID: 10218442.

[17] J. Yan, X. Meng, L.M. Wancket, K. Lintner, L.D. Nelin, B. Chen, K.P. Francis, C. V. Smith, L.K. Rogers, Y. Liu, Glutathione reductase facilitates host defense by sustaining phagocytic oxidative burst and promoting the development of neutrophil extracellular traps, J. Immunol. 188 (5) (2012) 2316–2327, https://doi.org/10.4049/jimmunol.1102683. PubMed PMID: 22279102; PMCID: PMC3480216.

[18] P.J. Halvey, W.H. Watson, J.M. Hansen, Y.M. Go, A. Samali, D.P. Jones, Compartmental oxidation of thiol-disulphide redox couples during epidermal growth factor signalling, Epub 2005/01/14, Biochem. J. 386 (Pt 2) (2005) 215–219, https://doi.org/10.1042/BJ20041829. PubMed PMID: 15647005; PMCID: PMC1134784.

[19] D.P. Jones, Redox potential of GSH/GSSG couple: assay and biological significance, Epub 2002/03/12, Methods Enzymol. 348 (2002) 93–112, https://doi.org/10.1016/s0076-6879(02)48630-2. PubMed PMID: 11885298.

[20] M. Velten, K.M. Heyob, L.K. Rogers, S.E. Welty, Deficits in lung alveolarization and function after systemic maternal inflammation and neonatal hyperoxia exposure, J. Appl. Physiol. 108 (5) (2010) 1347–1356. Epub 2010/03/13. doi: 01392.2009 [pii] 10.1152/japplphysiol.01392.2009. PubMed PMID: 20223995; PMCID: 2867533.

[21] H.Y. Cho, B. van Houten, X. Wang, L. Miller-Degraff, J. Fostel, W. Gladwell, L. Perrow, V. Panduri, L. Kobzik, M. Yamamoto, D.A. Bell, S.R. Kleeberger, Targeted deletion of Nrf2 impairs lung development and oxidant injury in neonatal mice, Epub 2012/03/10, Antioxidants Redox Signal. (2012), https://doi.org/10.1089/ars.2011.4288. PubMed PMID: 22400915.

[22] L. Flohe, The fairytale of the GSSG/GSH redox potential, Epub 2012/11/07, Biochim. Biophys. Acta 1830 (5) (2013) 3139–3142, https://doi.org/10.1016/j.bbagen.2012.10.020. PubMed PMID: 23127894.

[23] S.K. Berkelhamer, G.A. Kim, J.E. Radder, S. Wedgwood, L. Czech, R.H. Steinhorn, P.T. Schumacker, Developmental differences in hyperoxia-induced oxidative stress and cellular responses in the murine lung, Free Radic. Biol. Med. 61 (2013) 51–60, https://doi.org/10.1016/j.freeradbiomed.2013.03.003. PubMed PMID: 23499839; PMCID: PMC3723750.

[24] J.C. Lavoie, P. Chessex, Development of glutathione synthesis and gamma-glutamyltranspeptidase activities in tissues from newborn infants, Free Radic. Biol. Med. 24 (6) (1998) 994–1001. PubMed PMID: 9607610.

[25] S.K. Berkelhamer, K.N. Farrow, Developmental regulation of antioxidant enzymes and their impact on neonatal lung disease, Antioxidants Redox Signal. 21 (13) (2014) 1837–1848, https://doi.org/10.1089/ars.2013.5515. PubMed PMID: 24295375; PMCID: PMC4203145.

[26] J.H. Lindeman, E.G. Lentjes, H.M. Berger, Diminished protection against copper-induced lipid peroxidation by cord blood plasma of preterm and term infants, JPEN - J. Parenter. Enter. Nutr. 19 (5) (1995) 373–375, https://doi.org/10.1177/0148607195019005373. PubMed PMID: 8577014.

[27] J.H. Lindeman, E.G. Lentjes, D. van Zoeren-Grobben, H.M. Berger, Postnatal changes in plasma ceruloplasmin and transferrin antioxidant activities in preterm babies, Biol. Neonate 78 (2) (2000) 73–76, https://doi.org/10.1159/000014252. PubMed PMID: 10970997.

[28] C.C. Hsia, D.M. Hyde, M. Ochs, E.R. Weibel, Structure AEJTFoQAoL, An official research policy statement of the American Thoracic Society/European Respiratory Society: standards for quantitative assessment of lung structure, Epub 2010/02/05, Am. J. Respir. Crit. Care Med. 181 (4) (2010) 394–418, https://doi.org/10.1164/rccm.200809-1522ST. PubMed PMID: 20130146; PMCID: PMC5455840.

[29] R.W. Amy, D. Bowes, P.H. Burri, J. Haines, W.M. Thurlbeck, Postnatal growth of the mouse lung, J. Anat. 124 (Pt 1) (1977) 131–151. Epub 1977/09/01. PubMed PMID: 914698; PMCID: PMC1235518.

[30] S.I. Mund, M. Stampanoni, J.C. Schittny, Developmental alveolarization of the mouse lung, Epub 2008/07/25, Dev. Dynam. 237 (8) (2008) 2108–2116, https://doi.org/10.1002/dvdy.21633. PubMed PMID: 18651668.

[31] M. Herriges, E.E. Morrisey, Lung development: orchestrating the generation and regeneration of a complex organ, Epub 2014/01/23, Development 141 (3) (2014) 502–513, https://doi.org/10.1242/dev.098186. PubMed PMID: 24449833; PMCID: PMC3899811.

[32] J.C. Schittny, Development of the lung, Epub 2017/02/02, Cell Tissue Res. 367 (3) (2017) 427–444, https://doi.org/10.1007/s00441-016-2545-0. PubMed PMID: 28144783; PMCID: PMC5320013.

[33] J.H.T. Bates, Systems physiology of the airways in health and obstructive pulmonary disease, Wiley Interdisciplinary Reviews: Systems Biology and Medicine 8 (5) (2016) 423–437, https://doi.org/10.1002/wsbm.1347.

[34] J.L.Y. Cheong, L.W. Doyle, An update on pulmonary and neurodevelopmental outcomes of bronchopulmonary dysplasia, Epub 2018/11/08, Semin. Perinatol. 42 (7) (2018) 478–484, https://doi.org/10.1053/j.semperi.2018.09.013. PubMed PMID: 30401478.

[35] I. Narang, E. Baraldi, M. Silverman, A. Bush, Airway function measurements and the long-term follow-up of survivors of preterm birth with and without chronic lung disease, Epub 2006/04/18, Pediatr. Pulmonol. 41 (6) (2006) 497–508, https://doi.org/10.1002/ppul.20385. PubMed PMID: 16617446.

[36] E.G. Shepherd, B.J. Clouse, K.A. Hasenstab, S. Sitaram, D.T. Malleske, L.D. Nelin, S. R. Jadcherla, Infant pulmonary function testing and phenotypes in severe bronchopulmonary dysplasia, Epub 2018/04/07, Pediatrics 141 (5) (2018), https://doi.org/10.1542/peds.2017-3350. PubMed PMID: 29622720.

[37] P.J. Barnes, Reactive oxygen species and airway inflammation, Epub 1990/01/01, Free Radic. Biol. Med. 9 (3) (1990) 235–243, https://doi.org/10.1016/0891-5849(90)90034-g. PubMed PMID: 2272532.

[38] S.M. Orgeig, Janna, Lucy Sullivan, Christopher Daniels, in: R. Harding, K. Pinkerton (Eds.), Chapter 9- the Development of the Pulmonary Surfactant System, Academic Press, 2014.

[39] J.J. Batenburg, Surfactant phospholipids: synthesis and storage, Epub 1992/04/01, Am. J. Physiol. 262 (4 Pt 1) (1992) L367–L385, https://doi.org/10.1152/ajplung.1992.262.4.L367. PubMed PMID: 1566854.

[40] A.J. Ponsero, A. Igbaria, M.A. Darch, S. Miled, C.E. Outten, J.R. Winther, G. Palais, B. D'Autreaux, A. Delaunay-Moisan, M.B. Toledano, Endoplasmic reticulum transport of glutathione by Sec61 is regulated by Ero1 and bip, e5. Epub 2017/09/19, Mol Cell 67 (6) (2017) 962–973, https://doi.org/10.1016/j.molcel.2017.08.012. PubMed PMID: 28918898; PMCID: PMC5772773.

[41] S. Kotecha, A. Wangoo, M. Silverman, R.J. Shaw, Increase in the concentration of transforming growth factor beta-1 in bronchoalveolar lavage fluid before development of chronic lung disease of prematurity, Epub 1996/04/01, J. Pediatr. 128 (4) (1996) 464–469, https://doi.org/10.1016/s0022-3476(96)70355-4. PubMed PMID: 8618178.

[42] I. Mizikova, R.E. Morty, The extracellular matrix in bronchopulmonary dysplasia: target and source, Epub 2016/01/19, Front. Med. 2 (2015) 91, https://doi.org/10.3389/fmed.2015.00091. PubMed PMID: 26779482; PMCID: PMC4688343.

[43] S.A. McGrath-Morrow, T. Lauer, J.M. Collaco, A. Lopez, D. Malhotra, Y. O. Alekseyev, E. Neptune, R. Wise, S. Biswal, Transcriptional responses of neonatal mouse lung to hyperoxia by Nrf2 status, Epub 2013/10/22, Cytokine 65 (1) (2014) 4–9, https://doi.org/10.1016/j.cyto.2013.09.021. PubMed PMID: 24139870; PMCID: PMC3875154.

[44] G.T. Wagenaar, S.A. ter Horst, M.A. van Gastelen, L.M. Leijser, T. Mauad, P.A. van der Velden, E. de Heer, P.S. Hiemstra, B.J. Poorthuis, F.J. Walther, Gene expression profile and histopathology of experimental bronchopulmonary dysplasia induced by prolonged oxidative stress, Epub 2004/03/03, Free Radic. Biol. Med. 36 (6) (2004) 782–801, https://doi.org/10.1016/j.freeradbiomed.2003.12.007. PubMed PMID: 14990357.

[45] K. Lingappan, W. Jiang, L. Wang, B. Moorthy, Sex-specific differences in neonatal hyperoxic lung injury, Epub 2016/06/28, Am. J. Physiol. Lung Cell Mol. Physiol. 311 (2) (2016) L481–L493, https://doi.org/10.1152/ajplung.00047.2016. PubMed PMID: 27343189; PMCID: PMC5504425.

[46] C. Coarfa, Y. Zhang, S. Maity, D.N. Perera, W. Jiang, L. Wang, X. Couroucli, B. Moorthy, K. Lingappan, Sexual dimorphism of the pulmonary transcriptome in neonatal hyperoxic lung injury: identification of angiogenesis as a key pathway, Epub 2017/08/19, Am. J. Physiol. Lung Cell Mol. Physiol. 313 (6) (2017) L991–L1005, https://doi.org/10.1152/ajplung.00230.2017. PubMed PMID: 28818871; PMCID: PMC5814706.

[47] C.M. Alvira, Nuclear factor-kappa-B signaling in lung development and disease: one pathway, numerous functions, Epub 2014/03/19, Birth Defects Res A Clin Mol Teratol 100 (3) (2014) 202–216, https://doi.org/10.1002/bdra.23233. PubMed PMID: 24639404; PMCID: PMC4158903.

[48] S.N. Kazzi, U.O. Kim, M.W. Quasney, I. Buhimschi, Polymorphism of tumor necrosis factor-alpha and risk and severity of bronchopulmonary dysplasia among very low birth weight infants, Epub 2004/08/03, Pediatrics 114 (2) (2004) e243–e248, https://doi.org/10.1542/peds.114.2.e243. PubMed PMID: 15286263.